

Dynamics and thermodynamics of fragment emission from excited sources

M.J. Ison¹ and C.O. Dorso¹

¹ *Departamento de Física, Facultad de Ciencias Exactas y Naturales,
Universidad de Buenos Aires, Pabellón I, Ciudad Universitaria, Nuñez, 1428,
Buenos Aires, Argentina.*

(Dated: November 27, 2018)

In this paper we study the process of fragmentation of highly excited Lennard-Jones drops by introducing the concept of emitted fragments (clusters recognizable in configuration space which live more than a minimum lifetime). We focus on the dynamics and thermodynamics of the emitted sources, and show, among other things, that this kind of process can not be cast into a sequential or simultaneous one, and how a local equilibrium scenario comes up, allowing us to define and explore a local temperature, which turns out to be a strongly time-dependent quantity.

PACS numbers: 25.70.Mn, 25.70.-z, 25.70.Pq, 02.70.Ns

I. INTRODUCTION

The problem of fragmentation attracts the interest of physicists in many branches of physics. In particular, in this problem we have to deal with systems that are both finite and non-extensive. Moreover, we can face from extremely small systems like the nucleus to huge ones like galaxies. In both cases the size of the system under analysis is of the order of the range of the interaction potential and calls for a careful analysis. In what follows we will focus on the analysis of small Lennard-Jones (LJ) drops i.e. a system in which the dynamics is generated by a Hamiltonian in which there is a very short-range strong repulsion and a short-range attraction. As such we consider that it will give relevant insight into the problem of fragmentation.

This problem has been analyzed from different points of view and we classify them in two main groups i.e. Statistical models and dynamical models. In the first case [1] [2][3] the main assumption is that the fragmentation process is driven by phase-space occupancies. The always present assumption of *freeze-out* volume states that the system fragments in an equilibrium scenario at a given fixed volume and that thermal and chemical equilibrium is reached, in correspondence with the flavour chosen by the researcher (i.e. microcanonical, canonical or grand-canonical). Recently this kind of analysis has been extended to the isobaric isothermal ensemble [4]. Even in this kind of formulation there have been some efforts to include non-equilibrium effects, like for example the presence of expansive collective motion [5].

The other kind of models we dubbed, dynamical ones, include among others: Classical ones [6, 7, 8], quantum ones [9, 10], which are fully microscopic. In this category we also include those based on numerical realization of kinetic equations like BUU, VLD, etc. Focusing on the fully microscopic models the main advantage we find is that we have correlations of all orders at all times. Moreover non-equilibrium features of the process can be readily explored.

Continuing with a series of previous works we will

study the dynamics of highly excited 147 particles LJ drops [7]. Previously we have mainly considered the problem of fragment formation. We have shown that this phenomena takes place in phase space and as such it is not an experimental observable. In this communication we will focus our attention on the properties of the emitting sources and the corresponding emitted fragments. At this point it is worthwhile to define what we understand as emission. We say that a fragment has been emitted when it is recognizable in configuration space. We have already made this classification [11], and we have shown that there are well defined time scales for the processes of fragment formation and fragment emission.

In Section II we review the different fragment recognition algorithms currently in use. In Section III we present different Temperature definitions that will be relevant in the analysis of the evolution of the excited drops. Section IV deals with the model we study. Section V includes all the results we have obtained in our numerical simulations (fragment mass distributions, characteristic times, temperature of the emitting sources, role of the radial flux, etc). Finally conclusions will be drawn.

II. FRAGMENT RECOGNITION ALGORITHMS

The problem of analyzing molecular dynamics calculations is an old one and is not completely settled. To our knowledge there are three main fragment recognition algorithms in use: *MST*, *MSTE*, and *ECRA*.

The simplest and more intuitive cluster definition is based on correlations in configuration space: a particle i belongs to a cluster C if there is another particle j that belongs to C and $|\mathbf{r}_i - \mathbf{r}_j| \leq r_{cl}$, where r_{cl} is a parameter called the clusterization radius. If the interaction potential has a cut off radius r_{cut} , then r_{cl} must be equal or smaller than r_{cut} , in this work we chose $r_{cl} = r_{cut} = 3\sigma$. The algorithm that recognizes these clusters is known as the “Minimum Spanning Tree” (*MST*). The main drawbacks of this method is that only correlations in \mathbf{q} -space are used, neglecting completely the effect of momentum.

An extension of the MST is the “Minimum Spanning Tree in Energy space” (MSTE) algorithm [12]. In this case, a given set of particles i, j, \dots, k , belongs to the same cluster C_i if:

$$\forall i \in C_i, \exists j \in C_i / e_{ij} \leq 0 \quad (1)$$

where $e_{ij} = V(r_{ij}) + (\mathbf{p}_i - \mathbf{p}_j)^2 / 2\mu$, and μ is the reduced mass of the pair $\{i, j\}$. MSTE searches for configurational correlations between particles considering the relative momenta of particle pairs. In spite of not being supported by a physically-sound definition of a cluster, the MSTE algorithm typically recognizes fragments earlier than MST. Furthermore, due to its sensitivity in recognizing promptly emitted particles, it can be useful to study the pre-equilibrium energy distribution of the participant particles.

A more robust algorithm is based on the “Most Bound Partition” (MBP) of the system [13]. The MBP is the set of clusters $\{C_i\}$ for which the sum of the fragment internal energies attains its minimum value:

$$\begin{aligned} \{C_i\} &= \operatorname{argmin}_{\{C_i\}} [E_{\{C_i\}} = \sum_i E_{int}^{C_i}] \\ E_{int}^{C_i} &= \sum_i [\sum_{j \in C_i} K_j^{cm} + \sum_{\substack{j, k \in C_i \\ j \leq k}} V_{j, k}] \end{aligned} \quad (2)$$

where the first sum in (2) is over the clusters of the partition, K_j^{cm} is the kinetic energy of particle j measured in the center of mass frame of the cluster which contains particle j , and V_{ij} stands for the inter-particle potential. It can be shown that clusters belonging to the MBP are related to the most-bound density fluctuation in $\mathbf{r}-\mathbf{p}$ space [13].

The algorithm that finds the MBP is known as the “Early Cluster Recognition Algorithm” (ECRA). Since ECRA searches for the most-bound density fluctuations in $\mathbf{q}-\mathbf{p}$ space, valuable space and velocity correlations can be extracted at all times, specially at the very early stages of the evolution. This has been used extensively in many fragmentation studies [6, 7, 13, 14] and has helped to discover that excited drops break very early in the evolution.

When we use the three above-mentioned algorithms and we apply a criterium based on the average microscopic stability of the clusters (see for example [6]) to determine the corresponding times of fragment formation three time scales emerge, which satisfy the following relation: $\tau_{ECRA} < \tau_{MSTE} < \tau_{MST}$. But the meaning of each of these times is quite different. τ_{ECRA} refers to that time at which, on average, clusters attain microscopic stability regardless of the structure of the system in q -space. τ_{MSTE} has a rather obscure meaning because MSTE algorithm is not well defined from the physical point of view for dynamical problems. Finally τ_{MST} refers to that time at which, on average, microscopic stability is attained for free fragments. Please take into account that depending on the definition of r_{cl} this

last condition can be rephrased as “weakly interacting fragments”.

III. TEMPERATURES

Because we are aiming to perform some kind of thermodynamic analysis of the system, a prescription for the calculation of the temperature in small (and probably out of equilibrium) systems, is to be given. We should keep in mind that we are going to analyze physical processes in the framework of the molecular dynamics ensemble, which is the microcanonical ensemble plus the conservation of total momentum. Let us assume that at a given stage of the evolution of the system we can identify the biggest fragment according to *MST* algorithm.

In order to study the time evolution of the thermodynamics of the biggest emitting source we define the local temperature $T_{loc}(t)$ as the velocity fluctuations around the mean radial expansion of the biggest source. So we first introduce the mean radial velocity of the biggest source, which is defined as

$$v_{rad}(t) = \langle \frac{1}{N_{BF}} \sum_{i=1}^{N_{BF}} \frac{\mathbf{v}_i(t) \cdot \mathbf{r}_i(t)}{|\mathbf{r}_i(t)|} \rangle_e \quad (3)$$

Where N_{BF} indicates the number of particles of the biggest source at time t , and $\langle \rangle_e$ denotes an average over all events. Both $\mathbf{v}_i(t)$ and $\mathbf{r}_i(t)$ are measured from the center of mass of the biggest source. Taking into account that collective motion should not be considered to calculate the temperature, we define the local temperature as T_{loc} :

$$T_{loc}(t) = \frac{2}{3N_{BF}} \sum_{i=1}^{N_{BF}} \frac{m}{2} (\mathbf{v}_i(t) - v_{rad}(t) \cdot \hat{\mathbf{r}}_i(t))^2 \quad (4)$$

This definition is closely related to the one used in [6] for the analysis of expanding systems. In that case we obtained the local temperature of the system by the following procedure: We divided our drops in concentric spherical regions, centered in the c.m of the system, of width $\delta r = 2\sigma$. The mean radial velocity of region i in this case is:

$$v_{radshell}^{(i)}(t) = \frac{1}{N_i(t)} \sum_{ev} \sum_{j \in i} \frac{\mathbf{v}_j(t) \cdot \mathbf{r}_j(t)}{|\mathbf{r}_j(t)|} \quad (5)$$

where the first sum runs over the different events for a given energy, the second over the particles j that belong, at time t , to region i ; \mathbf{v}_j and \mathbf{r}_j are the velocity and position of particle j . $N_i(t)$ is total number of particles belonging to region i in all the events. Then the local temperature, which will be called $T_{shell}^{(i)}$, is defined as:

$$T_{shell}^{(i)} = \frac{2}{3} \frac{1}{N_i} \sum_{j \in i} \frac{1}{2} m \left(\mathbf{v}_j - \frac{v_{rad}^{(i)} \cdot \mathbf{r}_j}{|\mathbf{r}_j|} \right)^2 \quad (6)$$

where N_i is the total number of particles in cell i in all events.

The validity of Eq.4 and Eq.6 rely on the *conjecture* that the fragmenting system achieves local equilibrium (local equilibrium hypothesis). Whereas in the last case all particles in the inner shells should be equilibrated, the advantage of dealing with the local temperature (Eq.4) relies on the fact that only the biggest source is assumed to have reached some degree of equilibration. In this paper we will focus mainly on this definition. If the biggest source is assumed to have reached equilibrium, the velocity distribution should follow:

$$f(v) = \rho \left(\frac{m\beta}{2\pi} \right)^{3/2} e^{-\beta \frac{m}{2}(v-v_{rad})^2} \quad (7)$$

A first approach on the study of the local equilibrium hypothesis (LEH) consists in analyzing the isotropy of the velocity fluctuations around the expansion. For this purpose we introduce the radial and transversal local temperatures:

$$T_{loc}^{rad} = \frac{2}{N_{BF}} \sum_{i=1}^{N_{BF}} \frac{m}{2} [(\mathbf{v}_i(t) - v_{rad}(t) \cdot \hat{\mathbf{r}}_i(t)) \cdot \hat{\mathbf{r}}_i(t)]^2 \quad (8)$$

$$T_{loc}^{tra} = \frac{2}{N_{BF}} \sum_{i=1}^{N_{BF}} \frac{m}{2} [(\mathbf{v}_i(t) - v_{rad}(t) \cdot \hat{\mathbf{r}}_i(t)) \cdot \hat{\mathbf{r}}_{\perp i}(t)]^2 \quad (9)$$

A more profound analysis of the accuracy of the *LEH* is the study of the velocity distribution function and its comparison with (Eq.7). In order to perform this study we are to check the significance S of the fit of the distribution numerically obtained with the Eq.7. To address the question if both distributions are different we will perform a Pearson χ^2 test [15]. If the significance is high enough not to reject the hypothesis that both distributions differ we obtain as a by product the possibility of calculating the temperature as:

$$T_{max} = m\sigma^2 \quad (10)$$

Where σ is the width of the velocity distribution.

IV. THE MODEL

The system under study is composed, as in previous works, by $N = 147$ particles interacting via a truncated and shifted Lennard-Jones (*LJ*) potential, with a cut off radius $r_{cut} = 3\sigma$. Energies are measured in units of the potential well (ϵ), and the distance at which the *LJ* potential changes sign (σ), respectively. The unit of time used is $t_0 = \sqrt{\sigma^2 m / 48\epsilon}$.

The typical frequency of such potential is $\nu_0 \sim 0.2 \frac{1}{t_0}$. This defines a minimum time scale for the stability of an interacting system.

The equations of motion were integrated using the velocity Verlet algorithm, which preserves volume in phase space. We used an integration time step of $0.01t_0$, and performed a microcanonical sampling every $1t_0$ up to a final time of $t = 250t_0$.

This time scale was chosen because it has proven to be long enough as to the system to attain microscopic stability.

As stated in the previous section, we are mainly interested in the properties of fragments in configuration space. Then we are to analyze the *MD* evolutions using the *MST* algorithm. We define a fragmentation process when a source emits a stable fragment of at least 4 particles, i.e. the *MST* determination of fragments is complemented with a temporal stability condition. Otherwise we will be facing an evaporation process. The evolutions are analyzed in an event-by-event basis and the times at which fragmentation takes place are determined.

V. NUMERICAL EXPERIMENTS

Initial configurations are built as dense drops in q - *space* (region C of the phase diagram [16]). The total linear and angular momentum of the drops are removed and then, velocities are rescaled with a Maxwellian distribution so that the system has any desired value of total energy.

We covered a broad range of energies, namely -2.0ϵ , -1.0ϵ , -0.5ϵ , -0.2ϵ , 0.0ϵ , 0.2ϵ , 0.5ϵ , 1.0ϵ and 2.0ϵ (all reported energies are per particle). For each energy 1000 events were calculated.

A. Fragment mass distributions

The range of energies we used covers all regions of interest in multifragmentation. In Fig. 1, it can be clearly seen that the asymptotic mass distributions go from "U-shaped", at low energies to exponentially decaying ones, at high energies. Between these shapes a power-law (panel *b*) in Fig. 1 can be found. Technical details of the fitting procedure can be found elsewhere [17] but we would like to point out that the fitting procedure excludes the biggest fragment at each event, and also explicitly excludes monomers, dimers and trimers.

We have found interesting to study the multiplicity distribution of the number of times the system fragments for all events as a function of the energy of the system. In this case our approach is to follow the dynamics of the biggest source. At a given time $t_i = nt_0$ we identify the biggest *MST* fragment and check for the particles that belonged to this fragment at t_i , and formed a smaller cluster at $t = (n + 5)t_0$. We have chosen $5t_0$ as our threshold to accept the cluster as stable because that is of the order of the inverse of the natural frequency. In this way, we show in Fig.2 this distribution for energies per particle $E = -2.0\epsilon$, $E = 0.0\epsilon$, and $E = 2.0\epsilon$. It can be

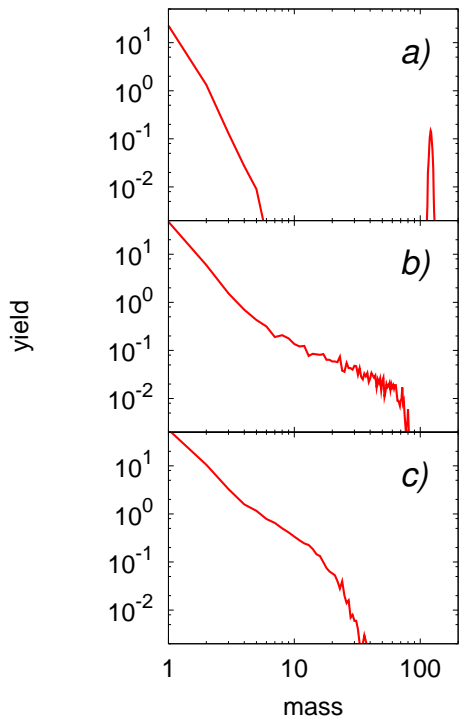


FIG. 1: Asymptotic mass spectra. Energies $E = -2.0\epsilon$, $E = 0.0\epsilon$, and $E = 2.0\epsilon$ are displayed in panels a), b), and c), respectively.

easily seen that, in this range of energy, as the energy of the system is increased, the maximum of the multiplicity distribution shifts towards higher values while the width of the distribution increases.

B. Characteristic times

Some discussion regarding the nature of the fragmentation process has focused on the distinction between simultaneous and sequential kind of phenomena. In our calculation the analysis of these kind of things are straightforward. Anyway, there are different characteristic times which can be explored. First we will look at the first and last time of emission. This means that we record for each of our evolutions the time at which the first fragmentation takes place according to the aboved-mentioned definition of an emission process. The result of that calculation are displayed in Fig.3.

We can see that at high energies ($E = 2.0\epsilon$) the distributions of times are narrower than at lower energies and does not seem to fit the view of a simultaneous process in configuration space (This issue will be further analyzed in Section V G). Another view of the same data is shown in Fig.4 in which what we show is the corresponding lapse of time between the first and last emission for each event. Once again, the distribution gets broader as the energy gets lower (the comparison should be restricted to events corresponding to $E = 0.0\epsilon$ and $E = 2.0\epsilon$ because of the

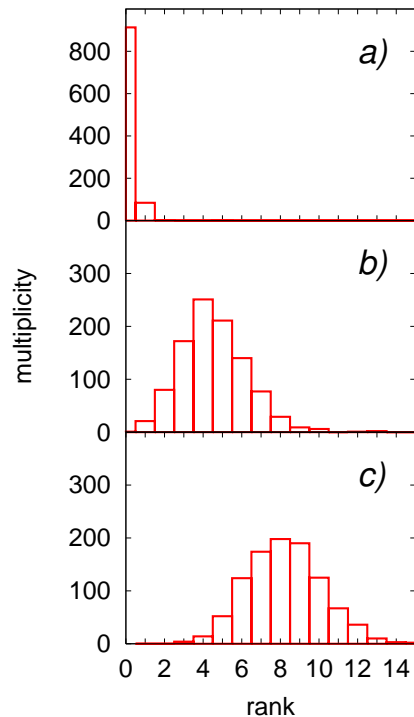


FIG. 2: Multiplicity distribution for $E = -2.0\epsilon$, $E = 0.0\epsilon$, and $E = 2.0\epsilon$ are shown in panels a), b), and c), respectively.

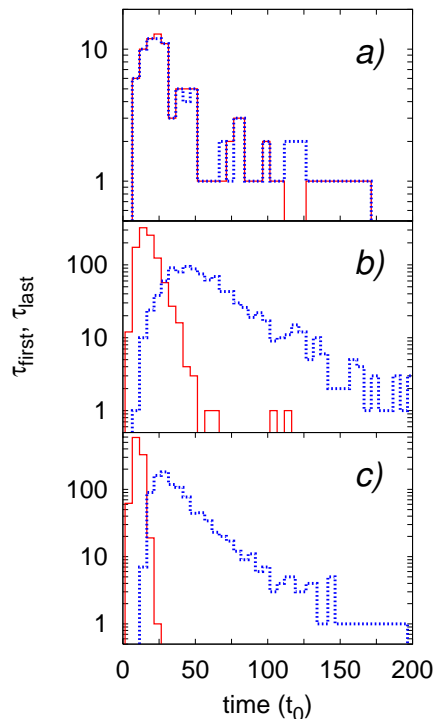


FIG. 3: (Color online) Distribution of first (full line) and last (dotted line) time of emission. Energies: $E = -2.0\epsilon$, $E = 0.0\epsilon$, and $E = 2.0\epsilon$ are displayed in panels a), b), and c), respectively.

very few emission processes that are found at $E = -2.0\epsilon$. In order to further illustrate the kind of process we are facing we show in Fig.5 the distribution of the mass of the emitting sources for the times of first and last emissions.

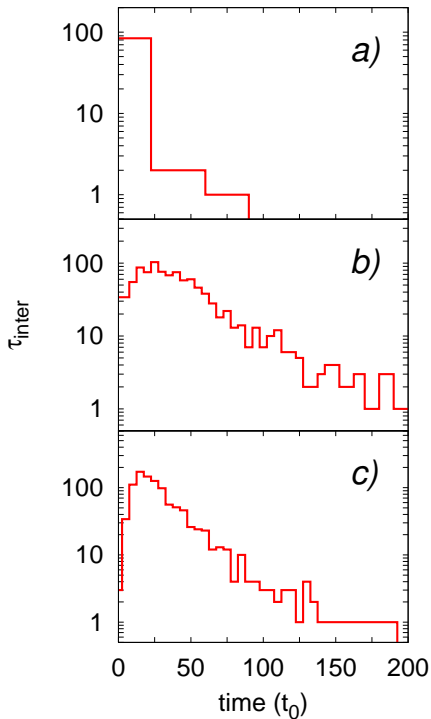


FIG. 4: Distribution of lapse of time between the first and last emissions. Energies: $E = -2.0\epsilon$, $E = 0.0\epsilon$, and $E = 2.0\epsilon$ are displayed in panels a), b), and c), respectively.

The most relevant issue of this figure is the presence, in panel b), of a broad range of masses at which the last emission takes place, since the value of energy ($E = 0.0\epsilon$) correspond to a power-law mass distribution.

The reason why we stated above that these results do not seem to fit the simultaneous emission picture without assuring it, is because we can also explore the possibility of occurrence of massive emission events. Even though emission events can be found in a rather large scale of time one may wonder if massive emission events have a definite characteristic time which would sustain the simultaneous picture.

We have used two definitions of "massive emission events (MEE)". The first one considers a MEE if the mass of the emitted fragment is at least 30% of the total mass of the biggest source at the time of emission. The second one states that a MEE has taken place if the mass of the biggest emitted fragment is at least composed of 40 particles. The results of such calculations are shown in Fig.6.

It is immediate that massive emission, according to definition 1, can take place at any time during the evolution, while when using the second definition (which is more restrictive) there are barely no massive events for

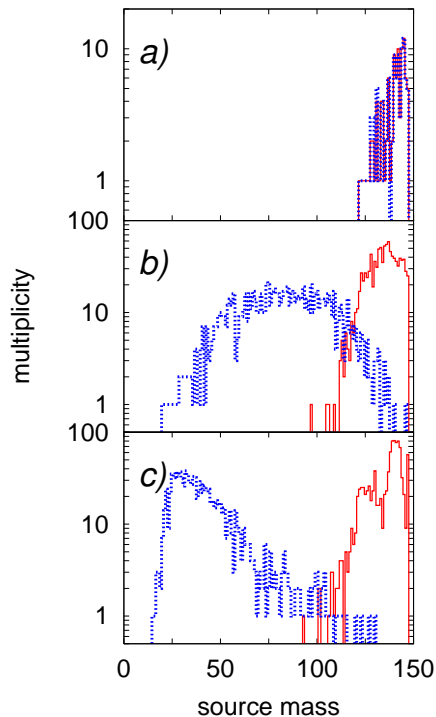


FIG. 5: (Color online) Distribution of mass of the emitting sources for the first (full line) and last (dotted line) emissions. Energies: $E = -2.0\epsilon$, $E = 0.0\epsilon$, and $E = 2.0\epsilon$ are displayed in panels a), b), and c), respectively.

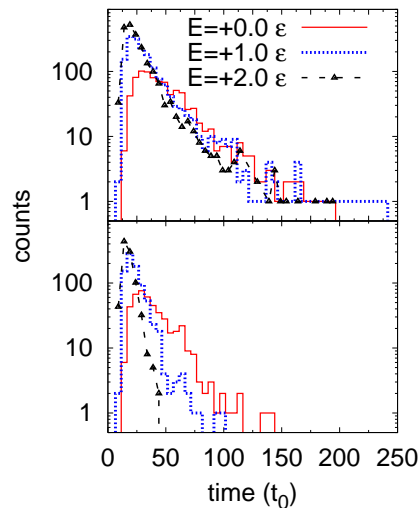


FIG. 6: (Color online) Distribution of emission times of massive fragments using criterium 1 (top) and criterium 2 (bottom); see text for details.

times greater than $t \sim 100t_0$. Also notice that the lower value of energy we used ($E = -2.0\epsilon$) is not present because no massive fragmentations were found.

In conclusion, when gathering all these results together we reach the conclusion that for the energies displayed in these figures the process can be viewed as a mixture of

sequential and simultaneous break up.

C. Temperatures of the emitting sources

It is natural to think that as the sources emit fragments they will undergo a cooling process. We should keep in mind that we are trying to analyze things in an event-by-event basis, without performing averages that would obscure the picture. In order to gain knowledge of the microscopic view of the fragmentation phenomena, we have calculated the evolution of the temperature, for a given energy and for each time step in which a fragmentation event takes place. The temperature is the one of the emitting source in the time step prior to the one in which the emission takes place. We then plot all this information in a single graph (see Fig.7).

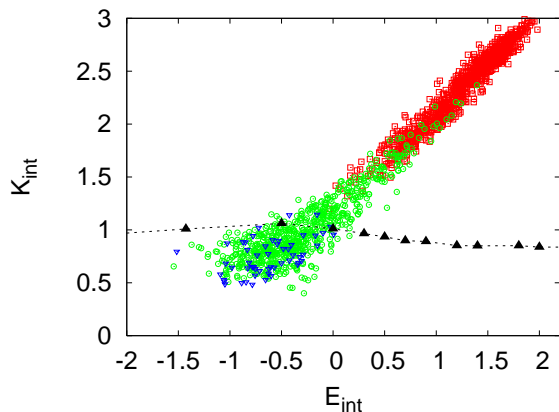


FIG. 7: (Color online) Internal kinetic energy of the emitting source as a function of its total internal energy for three ranks. Empty (red) squares denote 1st emission process. Empty (green) circles denote the 8th emission process, and empty (blue) triangles indicate the 12th emission process. Full (black) triangles stand for the caloric curve of the expanding system.

In Fig.7 we show the result for the analysis of 1000 events at an initial energy of $E = 2.0\epsilon$. In order to make the figure more readable we are only showing the above-described temperature for the first, last and maximum multiplicity fragmentation events. It is clearly seen that the internal kinetic energy is linear with the total internal energy and displays a cooling behavior. This overall behavior will not change if we consider not only fragmentation events but also evaporation events. It is interesting to notice that if one is to calculate temperatures from the analysis of the emitted light fragments (monomers, dimers, trimers) one would be sampling a source that starting from a rather high temperature, cools down monotonically. So the corresponding temperature should display a maximum at early times and decrease later on [18]. This is not a problem at all because the system is out of equilibrium and as such the

kind of measurements we are referring to at this point do not correspond to stable systems. What might be improper is to talk about temperature instead of "effective temperature". A more quantitative calculation is under progress and will be communicated shortly.

D. The role of radial flux

In a series of previous works [8] we have shown that, if the presence of collective (nonthermal) motion is not taken into account one find a wrong result: The presence of a vapor-branch in the caloric curve. Only when the radial flux is properly incorporated in the definition of the temperature one find that the nonequilibrium process of multifragmentation appears as an almost constant temperature region at high energies. In particular, in paper [11] we have calculated the time of fragment formation of this system, (using the ECRA phase-space method). The values of the mean radial velocity calculated for the biggest source in each event according to Eq.3 are shown in Fig.8.

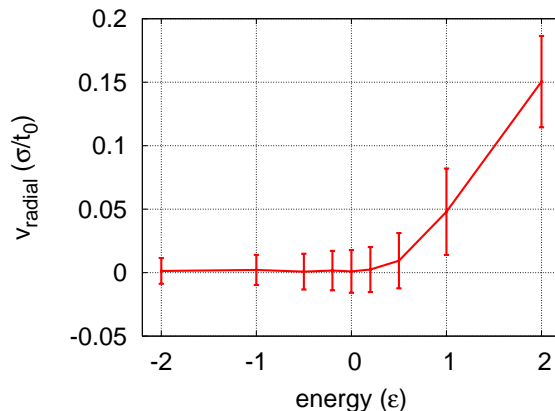


FIG. 8: Radial flux as a function of energy at time of fragment formation τ_{ff}

In Fig.9 we show the local temperature of the biggest source at time of fragment formation, as a function of the total energy (full line) The dotted line is included in order to emphasise the effect of not removing the radial collective motion when calculating caloric curves. As explained in Section III temperatures were calculated from velocity fluctuations around the collective motion.

In order to see how the picture emerging from a phase space analysis relates to the main topic of this paper i.e. the analysis in configuration space, we proceeded to calculate the temperature of the emitting sources at the stage of the evolution which correspond to the maximum of the multiplicity distribution (for example, looking at Fig.2b) the maximum of the distribution turns out to be rank=4). From this kind of analysis we get the empty circles of Fig.10. It can be easily seen that both approaches give the same temperature.

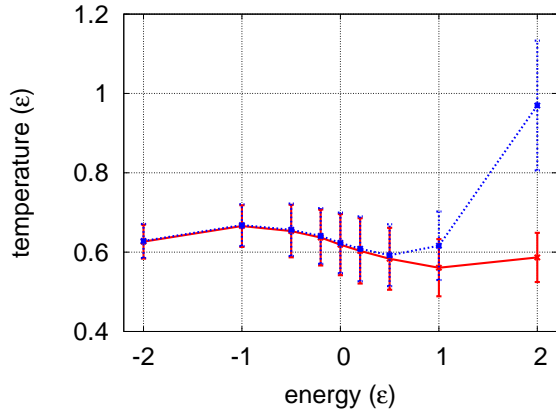


FIG. 9: (Local temperature) Local temperature of the biggest source at τ_{ff} (straight red line) and "fake temperature" (dotted blue line). The fake temperature is calculated from the total kinetic energy of the biggest source without taking into account the importance of the radial flux

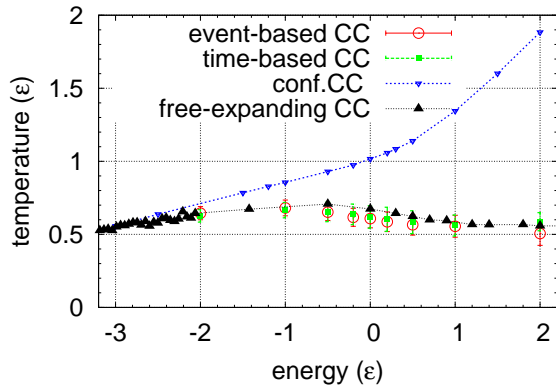


FIG. 10: (Color online) In this figure we show a comparison of caloric curves obtained by different thermometers. Empty circles correspond to an event-based temperature. Filled squares correspond to the temperature of the biggest source at time of fragment formation. Triangles up denote the local temperature (T_{shells}) and the dotted line with down triangles corresponds to the caloric curve obtained for a constrained system with a density $\rho = 0.17\sigma^{-3}$.

E. Local Equilibrium Hypothesis (LEH)

In previous sections we have made use of the hypothesis of local equilibrium.

In order to check this hypothesis we have performed the following calculation. Because in a local equilibrium scenario the fluctuations of velocity should be the same for the radial and transversal directions, we evaluated Eqs. 8 and 9, for a single event at the three energies chosen as examples in this work. In each of the three

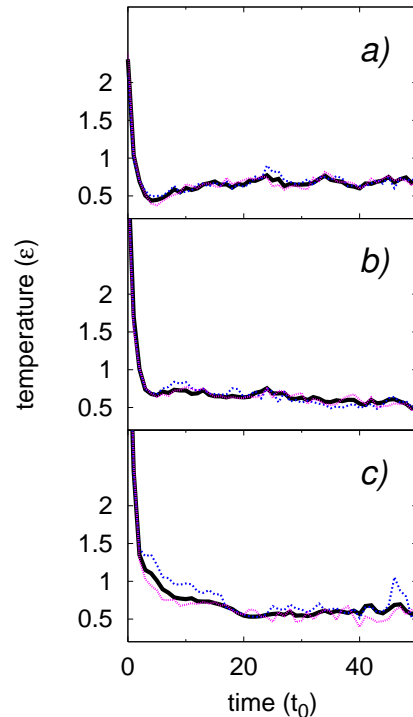


FIG. 11: (Color online) Radial (dotted line), transversal (thin line), and local (full line) temperatures of the biggest source for $E = -2.0\epsilon$ (panel a)), $E = 0.0\epsilon$ (panel b)), and $E = 2.0\epsilon$ (panel c))

panels of Fig.11, each corresponding to a different total energy (see caption for details), we show the three definitions of temperature above-mentioned. It is immediate that all of them are essentially the same, except for very early stages of the evolution (times much shorter than the time of fragment formation). This suggest that the the *LEH* at time of fragment formation seems plausible for all energies.

F. Maxwellian distribution of velocities

In this section we will show that the velocity distribution of the biggest source at time of fragment formation is indeed Maxwellian. Moreover, the temperature obtained from the standard deviation of the velocity distribution is almost exactly the same of Eq.4, showing the consistency of our numerical studies. In Fig.12 we show the histogram of the velocity distribution at time of fragment formation and its Maxwellian fit for $E = 2.0\epsilon$.

In addition to the excellent agreement between the velocity distributions and their fits we performed a Pearson χ^2 test, trying to reject the hypothesis that the distribution of velocities and that corresponding to the Maxwellian fit differ. We found a significance (S) above 0.25 for all cases, showing that, even with a very low confidence level like $CL = 0.80$ we could reject the hypothesis that both distributions differ (i.e. the velocity

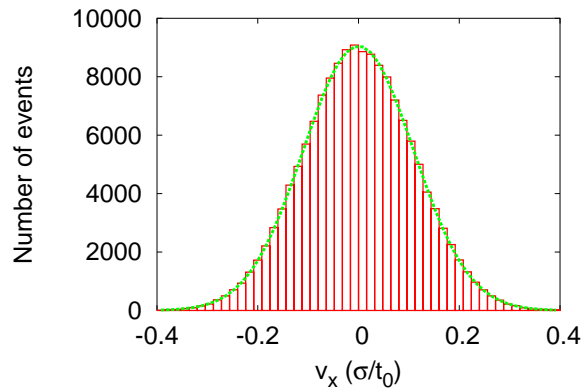


FIG. 12: (Color online) Velocity distribution (histogram) and Maxwellian fit (dotted line) for $E = +2.0\epsilon$

distribution is indeed Maxwellian).

TABLE I: Comparison of thermometers and statistical significance of the Maxwellian fit

$E(\epsilon)$	$T_{local}(\epsilon)$	$T_{fit}(\epsilon)$	$T_{event}(\epsilon)$	$T_{shell}(\epsilon)$	S
-2.0	0.627 ± 0.043	0.623	0.645	0.647	0.86
0.0	0.619 ± 0.077	0.630	0.608	0.674	0.82
2.0	0.587 ± 0.062	0.575	0.506	0.558	0.78

In Table.I we show a cross comparison of different thermometers. In addition to the already presented results we add the temperature obtained from the Maxwellian fit of the velocity distribution, and we also show the obtained statistical significance.

G. Reducibility

Not long ago, it has been proposed by Moretto and co-workers [19, 20] that the complex process of fragment emission could be described in terms of a binomial distribution. This approach rests on the assumption that a single transition probability p is capable of describing the emission process when no regard is pay to the mass or composition of the emitted fragments. In this way, the probability of emitting n fragments in a series of m trials should follow the well-known binomial distribution:

$$P_n^m = \frac{m!}{n!(m-n)!} p^n (1-p)^{m-n} \quad (11)$$

In which m stands for the number of "trials", while n stands for the number of successes. Following [19], we associate the parameter m to the maximum multiplicity for each energy and p stands for the transition probability. In Fig.13 we show the result of such an analysis. The

quality of the resulting fit is remarkable indeed, specially when one consider that we are facing an out of equilibrium non-simultaneous process while the very nature of the binomial process requires a constant value of p for the whole emission process.

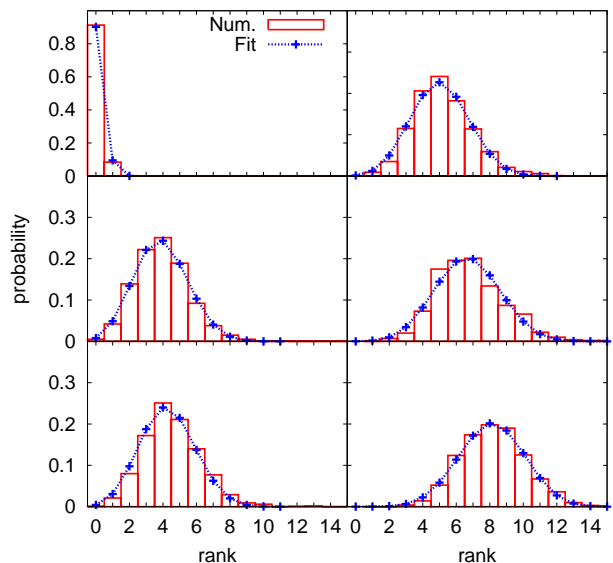


FIG. 13: (Color online) Multiplicity distribution (histograms) and binomial fit (dotted line). For energies (from top to bottom and left to right): $E = -2.0\epsilon$, $E = -0.2\epsilon$, $E = 0.0\epsilon$, $E = 0.2\epsilon$, $E = 1.0\epsilon$, and $E = 2.0\epsilon$

In order to further illustrate the accuracy of this approach we show in Fig.14 the calculated probability of emitting n fragments during the entire process as a function of the total energy, which $n = 0 - 5$. $P(n)$ is calculated assuming a binomial distribution (Eq. 11) with the value of p obtained from the best fit.

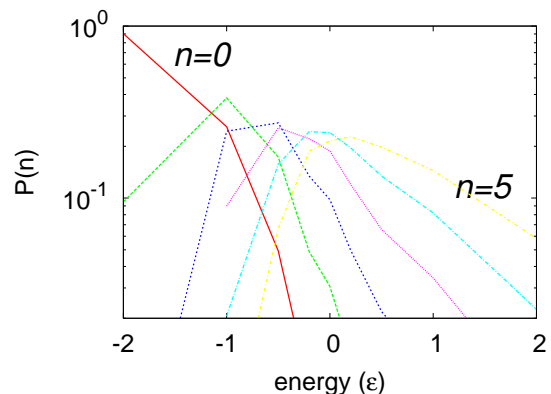


FIG. 14: (Color online) Probability of emitting 0 (red), 1 (green), 2 (blue), 3 (violet), 4 (cyan), 5 (yellow) fragments as a function of energy

We will not further analyze the implications of this binomial fit because we have not been able to calculate microscopically the associated transitions barriers yet.

VI. CONCLUSIONS

In this work we have analyzed the dynamics and thermodynamics of the emission process in a classical fragmenting system. We have focused on the evolution of the biggest source, and the corresponding emitted fragments. We have shown that the emission process can not be cast into a sequential nor into a simultaneous scenario, because even though there are many events in which fragments are emitted sequentially the phenomenon of massive emission is frequent enough as to forbid the characterization as a purely sequential one. We have also shown that when looking at fragments well defined in configuration space, the process of emission can not be cast into an isothermal one, i.e. temperatures are time-dependent. Moreover, there is a time-dependence of the size of the emitting source. As such, standard thermodynamical models which fix temperature and volume do not seem to be appropriate to reveal the true nature of the phenomenon under analysis. We have also shown, by analyzing the temperature of the source at the stage of most probable multiplicity, that it is possible to recover the caloric curve already obtained in the frame of phase-space analysis. If we recall Table I we see that temperature can be determined according to a few reasonable definitions, which provides in all cases consistent

results.

Two other interesting results have been obtained as a by-product of these calculations: First we should like to mention that the velocity distribution functions of the particles that form the biggest source are remarkably Maxwellian for times larger than the time of fragment formation after the collective expanding mode is removed. Second we have found that the probability of fragment emission (summed-up over all sizes) is amazingly binomial, suggesting a constancy of the transition amplitudes. We do not have a microscopic description of this constancy right now and we are currently working on it.

We hope that these findings will encourage the development of new, more accurate and realistic models to describe nuclear multifragmentation.

Acknowledgements

We acknowledge partial financial support from the University of Buenos Aires via grant X308. We also acknowledge partial financial support from CONICET (via grant PIP2304). C.O.D. is a member of the Carrera del Investigador (CONICET). M.J.I. is a fellow of UBA.

-
- [1] J. Randrup and S. E. Koonin *Nucl. Phys. A*, vol. 356, p. 223, 1981.
 - [2] J. B. Bondorf *et al. Phys. Reports*, vol. 257, p. 133, 1995.
 - [3] G. Fai and J. Randrup *Nucl. Phys. A*, vol. 381, p. 557, 1982.
 - [4] F. Gulminelli and P. Chomaz *Nucl. Phys. A*, vol. 734, p. 581, 2004.
 - [5] C. B. Das and S. D. Gupta *Phys. Rev. C*, vol. 64, p. 041601, 2001.
 - [6] A. Strachan and C. O. Dorso *Phys. Rev. C*, vol. 55, p. 775, 1997.
 - [7] A. Strachan and C. O. Dorso *Phys. Rev. C*, vol. 59, p. 285, 1999.
 - [8] A. Chernomoretz, M. Ison, S. Ortíz, and C. Dorso *Phys. Rev. C*, vol. 64, p. 024606, 2001.
 - [9] Y. Tosaka, A. Ono, and H. Horiuchi *Phys. Rev. C*, vol. 60, p. 064613, 1999. y referencias.
 - [10] J. Aichelin and H. Stoecker *Phys. Lett. B*, vol. 176, p. 14, 1986.
 - [11] A. Strachan and C. O. Dorso *Phys. Rev. C*, vol. 56, p. 995, 1997.
 - [12] X. Campi and H. Krivine *Nucl. Phys. A*, vol. 520, p. 46, 1997.
 - [13] C. O. Dorso and J. Randrup *Phys. Lett. B*, vol. 301, p. 328, 1993.
 - [14] A. Strachan and C. O. Dorso *Phys. Rev. C*, vol. 58, p. 632, 1998.
 - [15] W. Press, B. Flannery, S. Teukolsky, and W. T. Vetterling, *Numerical Recipes, The Art of Scientific Computing*. Cambridge University Press, 1989.
 - [16] A. Chernomoretz, P. Balenzuela, and C. Dorso *Nucl. Phys. A*, vol. 723, p. 229, 2003.
 - [17] P. Balenzuela, A. Chernomoretz, and C. Dorso *Phys. Rev. C*, vol. 66, p. 024613, 2002.
 - [18] J. B. Natowitz *et al. Phys. Rev. C*, vol. 65, p. 034618, 2002.
 - [19] L. G. Moretto, R. Ghetti, L. Phair, , K. Tso, and G. J. Wozniak *Physics Reports*, vol. 287, p. 249, 1997.
 - [20] L. G. Moretto, L. Phair, , K. Tso, and K. J. G. J. Wozniak *Nucl. Phys. A*, vol. 583, p. 513, 1995.